where $\delta n_{1,2}$ = (sin 54.7°) $\delta\theta_{1,2}$ and using the first-order expansion analogous to A8 we "solve" eq 12–14 as

$$d_{22} = \frac{3(2^{1/2})}{4}(\sin 54.7^\circ)V^{-1}(\beta_{33} - 3\beta_{31})(\delta\theta_1 + \delta\theta_2) \quad \text{(A18)}$$

$$d_{33} = -3(\sin 54.7^\circ)V^{-1}\beta_{33}(\delta\theta_1 + \delta\theta_2) \quad \text{(A19)}$$

$$d_{31} = -3(\sin 54.7^\circ)V^{-1}\beta_{31}(\delta\theta_1 + \delta\theta_2) \quad \text{(A20)}$$

Registry No. $NaIO_4 \cdot 3H_2O$, 13872-31-6; $NaH_3O[IO_3(OH)_3]$, 34410-79-2.

References and Notes

(1) J. G. Bergman and G. R. Crane, *Chem. Phys. Lett.*, **41**, 133–136 (1976).
(2) G. R. Crane and J. G. Bergman, *J. Appl. Crystallogr.*, **9**, 476 (1976).
(3) J. G. Bergman and J. S. Wood, *J. Chem. Soc., Chem. Commun.*, 457 (1976).
(4) J. G. Bergman, *J. Am. Chem. Soc.*, **98**, 1054 (1976).
(5) H. Poulet and J. P. Mathieu, *J. Raman Spectrosc.*, **2**, 81–92 (1974).
(6) J. F. Nye, "Physical Properties of Crystals", Oxford University Press, London, 1957.
(7) F. G. Parsens, E. Y. Chen, and R. K. Chang, *Phys. Rev. Lett.*, **27**, 1436 (1971).
(8) D. A. Kleinman, *Phys. Rev.*, **126**, 1977 (1962).
(9) R. J. W. LeFèvre, *Adv. Phys. Org. Chem.*, **3**, 1–90 (1965).
(10) A. D. Buckingham and B. J. Orr, *Q. Rev., Chem. Soc.*, **21**, 195, (1976).
(11) F. N. H. Robinson, *Bell Syst. Tech. J.*, **46**, 913 (1967).
(12) J. G. Bergman and G. R. Crane, *J. Chem. Phys.*, **60**, 2470–2474 (1974).
(13) J. G. Bergman, Jr., and S. K. Kurtz, *Mater. Sci. Eng.*, **5**, 235–250 (1969/70).
(14) R. Burgers, *Proc. R. Soc. London, Ser. A*, **116**, 553–586 (1927).
(15) G. D. Boyd, H. Kasper, and J. H. McFee, *IEEE J. Quantum Electron.*, **QE-7**, 563–573 (1971).
(16) G. R. Crane, *J. Appl. Phys.*, **44**, 915–196 (1973).
(17) J. Jerphagnon and S. K. Kurtz, *Phys. Rev.*, **113**, 1738–1744 (1970).
(18) E. S. Larsen and H. Berman, *U.S. Geol. Surv., Bull.*, **No. 848**, 254 (1934).
(19) J. L. Bernstein, S. C. Abrahams, and F. Lissalde, submitted for publication.
(20) We note here that this expression has absorbed local field corrections and hence β is an "effective bond polarizability".
(21) The polarizability of eq 7 is given in a coordinate system where $\hat{z}$ is the symmetry axis.

Contribution from the Department of Chemistry, University of Berne, CH-3000 Berne 9, Switzerland

Jahn–Teller Effect in the $^4T_{2g}$ State of Chromium(III) in Dicesium Sodium Indium(III) Hexachloride

HANS U. GÜDEL* and TIMOTHY R. SNELLGROVE

Received September 12, 1977

Low-temperature absorption and luminescence spectra are reported for the $^4A_{2g} \leftrightarrow {}^4T_{2g}$ transition of $CrCl_6^{3-}$ doped into the elpasolite salt $Cs_2NaInCl_6$. Four magnetic dipole origins are assigned at 11 882, 11 890, 11 904, 11 916 cm^{-1}, and the vibronic sidebands of the luminescence spectra are assigned to progressions in a_{1g} and e_g modes on t_{1u} and t_{2u} false origins with frequencies 297, 240, 187, and 120 cm^{-1}. The splitting of the $^4T_{2g}$ state is smaller than expected from calculations using the full d^3 matrix. Using the effective Hamiltonian formalism, we show that the splittings may be reproduced by introducing a Ham reduction factor for off-diagonal matrix elements of $\hat{H}_{eff}$. The Jahn–Teller interaction is compatible with the presence in the luminescence of a progression in the e_g (Jahn–Teller active) mode. The Jahn–Teller energy calculated from the observed splittings is 310 cm^{-1} and that from intensity ratios in the e_g progression 264 cm^{-1}, justifying the treatment of the spin–orbit interaction as small compared with E_{JT}.

Introduction

The elpasolite salts Cs_2NaMCl_6, containing octahedral MCl_6^{3-} complexes, are useful high-symmetry host lattices for the study of trivalent transition-metal ions. The visible and MCD spectra of Cr^{3+} doped into Cs_2NaYCl_6 and $Cs_2NaInCl_6$ have been extensively studied.[1,2] In $CrCl_6^{3-}$ the value of Dq is low and the $^4T_{2g}$ state is found to be the first excited state, 12 000 cm^{-1} above the $^4A_{2g}$ ground state. We have obtained the luminescence spectrum of this transition and the absorption spectrum of a thick crystal in the same region. The $^4T_{2g}$ state splits into E′, U′($^5/_2$), U′($^3/_2$), and E″ states under the influence of spin–orbit coupling. The MCD and absorption spectra are thus complicated superpositions of the vibronic intensity from all four transitions whereas the luminescence spectrum at low temperature contains only vibronic structure from the lowest energy electronic transition. The sensitivity of the luminescence experiment is such that we can measure the vibronic spectrum due to lattice modes in the crystal.

In spite of the observation of progressions in the e_g mode as well as the a_{1g} mode of $CrCl_6^{3-}$ in the MCD spectra, previous work has neglected the Jahn–Teller interaction in the interpretation of this transition. We find our results can only be explained by considerable quenching of the spin–orbit interaction due to the Ham effect, as observed in other T_{2g} and T_{1g} states of octahedral 3d ions.[3,4]

Experimental Section

$Cs_2NaInCl_6$:Cr was kindly prepared by Woodwark.[5] The crystal was grown by the Bridgeman technique. Analysis for chromium using atomic absorption spectroscopy showed a concentration around 5 atom %. The boule contains a considerable percentage of Cr^{2+},[6] which we observe as a strong broad band in the near-IR absorption spectrum. The Cr^{3+} concentration may well be less than 5%. Absorption spectra were measured on 2 and 5 mm thick crystals with a Cary 17 spectrophotometer, equipped with a red-sensitive photomultiplier tube (RCA C31025C). Luminescence spectra were excited with a 150-W sealed-beam Xe arc (Varian) filtered with a Spex Minimate. The luminescence was dispersed with a $^3/_4$-m single Spex monochromator, with a grating blazed at 750 nm. An EMI 9684B photomultiplier (S1 response) cooled to −70 °C was used to detect the luminescence. High-resolution spectra were recorded between 830 and 880 nm using a RCA C31034 photomultiplier cooled to −30 °C. The crystals were cooled using a helium gas flow technique.

Results

Figure 1 shows the broad-band luminescence spectrum. We assign this in terms of the weak pure electronic transitions, two strong vibronic false origins, and progressions in a_{1g} and e_g modes. Figures 2 and 3 show the detailed absorption and luminescence spectra in the region where these overlap. The four bands at 11 882, 11 890, 11 904, and 11 916 cm^{-1} are found in absorption and luminescence spectra. The oscillator strengths in absorption are 1.6, 1.6, 0.9, and 0.9 × 10^{-9} for the four origins. In the luminescence spectrum the intensities vary with temperature according to a Boltzmann distribution among levels at 0, 8, 21, and 34 cm^{-1}. The vibronic sideband at the right of Figure 3 shows a similar temperature dependence, hot bands appearing at the high-energy side of the band with equal spacing and similar relative intensity as the origins. The second intense false origin at 187 cm^{-1} gives a similar pattern. We cannot assign the hot bands in the lu-

0020-1669/78/1317-1617$01.00/0

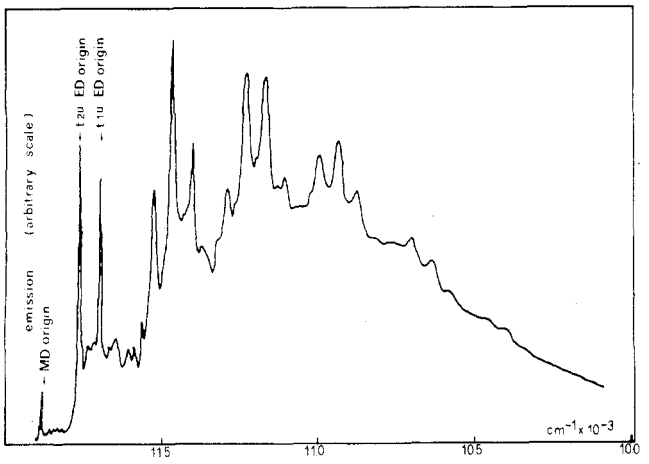

Figure 1. The 10 K luminescence spectrum of $Cs_2NaInCl_6:Cr^{3+}$. No correction was applied for monochromator and photomultiplier response (S1).

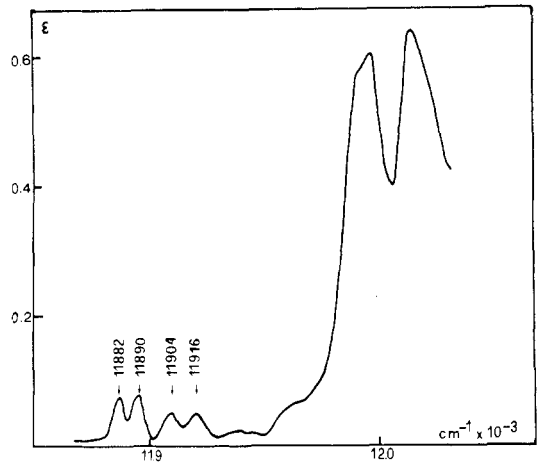

Figure 2. The 8 K absorption spectrum in the region of the $^4A_{2g} \rightarrow {}^4T_{2g}$ origins in $Cs_2NaInCl_6:Cr^{3+}$.

Table I. Vibrational Frequencies (cm^{-1}) in MCl_6^{3-} Systems[a]

	$Cs_2NaCrCl_6$[2]	$Cs_2NaInCl_6$[2]	$Cs_2NaYCl_6:Cr^{3+}$ $^4T_{2g}$[1]	$Cs_2NaLaCl_6$[6]
a_{1g}		294 R	300 Abs, MCD	
e_g			240 MCD	236 R
t_{2g}		139 R		
t_{1u}	195 IR		195 MCD	
t'_{1u}	320 IR			
t_{2u}			130 MCD	

[a] Key: IR, infrared spectroscopy; R, Raman spectroscopy; Abs, absorption spectroscopy; MCD, magnetic circular dichroism.

minescence spectrum as due to vibronic levels since the corresponding cold bands are not observed. We therefore assign the four lowest energy bands in absorption as the magnetic dipole origins of the $^4A_{2g} \rightarrow {}^4T_{2g}$ transition. This assignment is supported by the coincidence of the four lines in absorption and luminescence.

Turning to the vibronic structure in Figure 1, we present the measured vibrational frequencies in this and related systems in Table I. Frequencies have been assigned assuming the vibrations of $CrCl_6^{3-}$ may be treated in isolation as local modes of the crystal. We see that the frequencies do not vary much between ground and excited states in $CrCl_6^{3-}$.

The origin is followed by a number of weak bands probably involving lattice modes of the crystal (Table II). The two prominent bands positioned 120 and 187 cm^{-1} away from the origin are assigned as the t_{2u} and t_{1u} false origins. The t'_{1u} mode does not appear to couple strongly with the electronic transition but we find a band 323 cm^{-1} from the origin which could be due to this vibration. The pattern of lattice modes found on the origin is found also coupled to the t_{1u} and t_{2u} false origins; the intensity pattern is somewhat disturbed in the case of the t_{1u} mode. The presence of the e_g vibronic band with

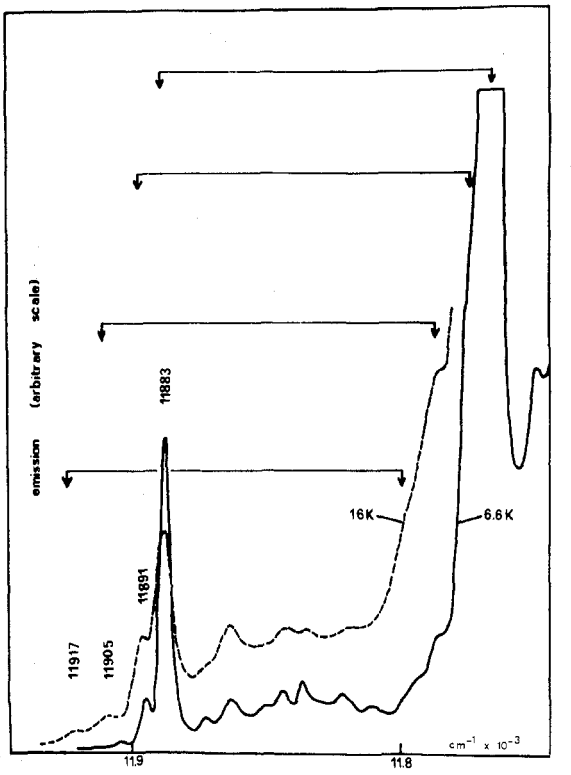

Figure 3. Detailed luminescence spectrum in the region of the $^4T_{2g} \rightarrow {}^4A_{2g}$ origins in $Cs_2NaInCl_6:Cr^{3+}$. The temperature dependence of the electronic origins is reproduced in the vibronic sideband system at the right-hand side.

Table II. Vibronic Analysis of 10 K Luminescence Spectrum of $Cs_2NaInCl_6:Cr^{3+}$

Posn, $cm^{-1} \times 10^{-3}$	Assign[a]	Posn $cm \times 10^{-3}$	Assign
11 883	MD origin	11 585	a_{1g}
11 867	LM 16 cm^{-1}[b]	11 559	t'_{1u}
11 858	LM 25 cm^{-1}	11 552	$t_{2u} + e_g$
11 845	LM 38 cm^{-1}	11 463	$t_{2u} + a_{1g}$
11 838	LM 45 cm^{-1}	11 452	$t_{1u} + e_g$
11 831	LM 52 cm^{-1}	11 397	$t_{1u} + a_{1g}$
11 816	LM 67 cm^{-1}	11 285	$t_{2u} + 2e_g$
11 806	LM 77 cm^{-1}	11 225	$t_{1u} + 2e_g$
11 763	t_{2u}		$t_{2u} + e_g + a_{1g}$
11 744	LM 19 cm^{-1}	11 161	$t_{2u} + 2a_{1g}$
11 736	LM 27 cm^{-1}		$t_{1u} + e_g + a_{1g}$
11 728	LM 35 cm^{-1}	11 099	$t_{1u} + 2a_{1g}$
11 722	LM 41 cm^{-1}	10 990	$t_{2u} + 2e_g + a_{1g}$
11 716	LM 47 cm^{-1}	10 927	$t_{2u} + e_g + 2a_{1g}$
11 709	LM 54 cm^{-1}	10 866	$t_{1u} + e_g + 2a_{1g}$
11 696	t_{1u}		$t_{2u} + 3a_{1g}$
11 682	LM 14 cm^{-1}	10 692	$t_{2u} + 2e_g + 2a_{1g}$
11 671	LM 25 cm^{-1}	10 630	$t_{2u} + e_g + 3a_{1g}$
11 659	LM 37 cm^{-1}	10 569	$t_{1u} + e_g + 3a_{1g}$
11 652	LM 44 cm^{-1}		$t_{2u} + 4a_{1g}$
11 645	LM + e_g	10 331	$t_{2u} + e_g + 4a_{1g}$
11 606			

[a] The main features in the spectrum can be rationalized considering only the following four vibrations of the octahedral $CrCl_6^{3-}$ unit in the ground state: $t_{2u} = 120$ cm^{-1}, $t_{1u} = 187$ cm^{-1}, $e_g = 240$ cm^{-1}, $a_{1g} = 298$ cm^{-1}. [b] Bands assigned to lattice modes are designated LM followed by the frequency shift from the band from which they are derived.

Table III. Spin–Orbit Components of $^4T_{2g}$ in $CrCl_6^{3-}$

E′	107[a]	106[b]	34[c]	32[d]
U′($^5/_2$)	82[a]	81[b]	22[c]	24[d]
U′($^3/_2$)	36[a]	35[b]	8[c]	9[d]
E″	0[a]	0[b]	0[c]	0[d]

[a] Calculation using full d^3 matrix with $B = 570$, $C = 3420$, $Dq = 1300$, and $\zeta = 170$ cm^{-1}. [b] Calculation using $\hat{H}_{eff}$ with $\lambda = -24$, $\kappa = 5$, and $\rho = -15$ cm^{-1}. [c] Observed. [d] Calculation with Jahn–Teller interaction (Jahn–Teller energy 310 cm^{-1}).

a frequency of 239 cm^{-1} coupled to the origin would explain this, since it would fall in the same position as a lattice mode. Finally, we find the a_{1g} mode coupled to the origin with a frequency of 297 cm^{-1}. The intensity of the t_{1u} and t_{2u} false origins agrees with the interpretation of the temperature dependence of the absorption of $^4A_{2g} \rightarrow {}^4T_{2g}{}^1$ and an analysis of the MCD spectra[2] where the activity of both modes with approximately equal intensity is postulated.

The remaining structure in the spectrum may be explained by progressions in a_{1g} (298 cm^{-1}) and e_g (240 cm^{-1}) built on the t_{1u} and t_{2u} false origins (Table III). The progression in a_{1g} dominates, but we find up to two members of the progression in e_g based on the t_{1u} false origin and elsewhere at least the first member. Measuring intensity in the e_g progression is difficult since the choice of baseline is somewhat arbitrary, but the $0 \rightarrow 0$ transition is usually as intense as the $0 \rightarrow 1$ transition. In the case of the t_{2u} false orgin, we measure the following intensity ratios: $0 \rightarrow 1/0 \rightarrow 0$, 1.1; $0 \rightarrow 2/0 \rightarrow 1$, 0.6.

We regard the identification of the origins, the t_{2u} and t_{1u} false origins, and the progressions in a_{1g} and e_g as certain. The remaining structure is more difficult to assign. Our interpretation does explain most of the spectrum.

Theoretical Discussion

(a) Ham Quenching of Spin–Orbit Splitting in $^4T_{2g}$. The case of a T_{1g} or T_{2g} electronic state coupled to an e_g vibrational mode in O_h symmetry has been treated by Ham[7] and Sturge.[3] We follow the treatment of Sturge. The Jahn–Teller effect will be treated as larger than the spin–orbit interaction, and all anharmonic effects will be neglected. We consider coupling only with the e_g mode; there is no experimental evidence for coupling with the t_{2g} mode and such coupling is expected to be weak in a $t_{2g}{}^2e_g$ configuration.[8]

As basis functions we shall use the eigenfunctions of

$$\hat{H} = \hat{H}_{e/r_{12}} + \hat{H}_{cubic} \tag{1}$$

The spin–orbit coupling is treated to second order using the effective Hamiltonian

$$\hat{H}_{eff} = -\lambda(\hat{L}\cdot\hat{S}) + \kappa(\hat{L}\cdot\hat{S})^2 + \rho(\hat{L}_x{}^2\cdot\hat{S}_x{}^2 + \hat{L}_y{}^2\cdot\hat{S}_y{}^2 + \hat{L}_z{}^2\cdot\hat{S}_z{}^2) \tag{2}$$

Values of λ, κ, and ρ are determined by diagonalizing the full matrix for d^3 including the spin–orbit interaction and fitting the calculated splittings in $^4T_{2g}$ with $\hat{H}_{eff}$. The full matrix was calculated with the following parameters: $B = 570$, $C/B = 6$, $Dq = 1300$, $\zeta = 170$ cm^{-1}. The parameters were chosen to correspond with the literature[1,2,9] and in particular to reproduce the observed splitting between $^4T_{2g}$ and ^2E_g which have a large second-order interaction. The calculated energies of the spin–orbit components are given in Table III; the observed splittings are smaller which we interpret as a Ham effect. To first order in $\hat{L}\cdot\hat{S}$, E′ and U′($^5/_2$) are degenerate; the splitting of the levels is due to the large second-order interactions. The calculated levels may be fitted with $\hat{H}_{eff}$ using $\lambda = -24$, $\kappa = 5$, and $\rho = -15$ cm^{-1} (Table III).

We use the notation $|i\rangle$, $i = \xi, \eta, \zeta$, for the components of T_{2g} and Q_2 and Q_3 to represent the coordinates of the e_g mode.

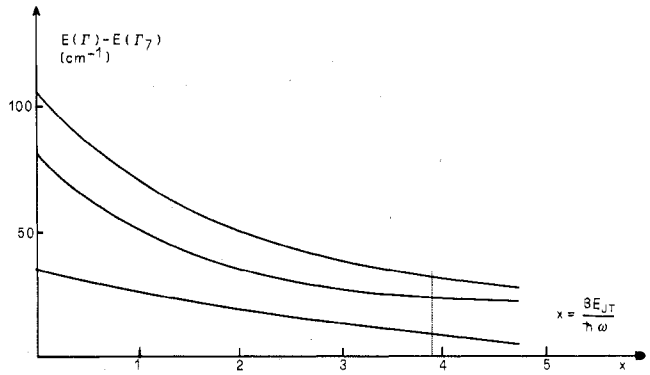

Figure 4. Spin–orbit splittings and Jahn–Teller effect in the $^4T_{2g}$ state. The splitting at the left-hand side of the diagram is obtained by diagonalizing $\hat{H}_{eff}$ (eq 2) with the following parameters: $\lambda = 24$, $\kappa = 5$, and $\rho = -15$ cm^{-1}. The dotted line ($x = 3.9$) represents the best fit with the experimentally observed splitting. $\Gamma_7 \simeq E''$.

The Jahn–Teller Hamiltonian acting on (ξ, η, ζ) may be written

$$\hat{H}_{JT} = \frac{1}{2\mu}\sum_{k=2,3}(-\hbar^2\partial/\partial Q_k{}^2 + \mu^2\omega^2Q_k{}^2) - VQ_2\begin{bmatrix} 3^{1/2}/2 & 0 & 0 \\ 0 & -3^{1/2}/2 & 0 \\ 0 & 0 & 0 \end{bmatrix} - VQ_3\begin{bmatrix} -1/2 & 0 & 0 \\ 0 & -1/2 & 0 \\ 0 & 0 & 1 \end{bmatrix} \tag{3}$$

where μ is the effective mass in the e_g mode, ω is the angular frequency, and V is the Jahn–Teller parameter. This Hamiltonian is diagonal in the components of T_{2g}. For the lowest vibrational state the vibrational function splits into three parabolic potential wells, one for each component of T_{2g}. The minima of the potential functions are displaced in (Q_2, Q_3) space from the origin in the absence of a Jahn–Teller effect ($V = 0$). The displacement is

$$\rho_i(Q_2) = -\frac{V}{\mu\omega^2}E_i(Q_2) \qquad \rho_i(Q_3) = -\frac{V}{\mu\omega^2}E_i(Q_3) \tag{4}$$

where $E_i(Q_k)$ is the matrix element corresponding to $|i\rangle$ and Q_k in eq 3. The energy minimum is lower than in the undistorted case by $E_{JT} = V^2/2\mu\omega^2$. The wave functions may be written

$$|inm\rangle = |i\rangle F_n(Q_2 + \rho_i(Q_2))F_m(Q_3 + \rho_i(Q_3)) \tag{5}$$

The F_n are standard harmonic oscillator functions; n and m are the quantum numbers of the vibration.

The Ham effect arises when we consider integrals between the components of $^4T_{2g}$:

$$\langle j M_S' 00|H_{eff}|i M_S 00\rangle = \langle j M_S'|H_{eff}|i M_S\rangle \times (\delta_{ij} + \gamma(1 - \delta_{ij})) \tag{6}$$

where γ, the Ham reduction factor, is $e^{-x/2}$ and $x = 3E_{JT}/\hbar\omega$. Because the vibrational functions differ for $i \neq j$, the overlap is no longer 1 but reduced by γ.

The matrix of $\hat{H}_{eff}$ was diagonalized including (6). Off-diagonal elements due to the Jahn–Teller interaction were neglected since they are small in this case.[3] The results for various values of x are shown in Figure 4. The best fit is obtained with $x = 3.9$ corresponding to a Ham quenching factor of 0.14. The calculated splittings are given in Table III.

(b) e_g Progression in Luminescence Spectrum. The intensity in the luminescence spectrum depends on the transition moments between ground and excited states which take the form $|\langle a\, nm|\hat{M}|i\, 00\rangle|$, where $\langle a\, nm|$ is the ground state and $\hat{M}$ is any transition moment operator. The vibrational functions in the ground state are undistorted. Assuming

harmonic potential wells and no change in force constant between ground and excited states, the intensity of the vibronic transitions in low-temperatre luminescence depends on the overlap integrals $\langle F_0(Q_2 + \rho_i(Q_2)) | F_n(Q_2) \rangle$. The situation is analogous to a Frank–Condon progression in an a_{1g} mode, and the combination of Q_2, Q_3 which gives rise to the Jahn–Teller distortion has a_{1g} symmetry in the lower symmetry of the distorted molecule. To calculate the relative intensity in each member of the progression we may use the formula

$$I_n = \frac{1}{n}\left(\frac{x}{3}\right)^2 I_{n-1} \qquad n = \text{number of quanta of } e_g \qquad (7)$$

adapted from Ballhausen.[10] In fact we measure intensities in the progressions based on the t_{1u} and t_{2u} false origins. Since these modes are diagonal in H_{JT}, we can apply the same analysis. For $x = 3.9$, the value obtained from the quenching of spin–orbit splitting, the intensity ratios I_1/I_0 or I_2/I_1 are 1.3 and 0.85 which are in reasonable agreement with experiment. The best agreement in the case of the t_{2u} false origin is found for $x = 3.3$ giving intensity ratios 1.1 and 0.6.

The Jahn–Teller energy calculated from the observed spin–orbit splitting is 310 cm^{-1} ($x = 3.9$) and that from the intensity ratios in the e_g progression 264 cm^{-1} ($x = 3.3$). Both values are considerably larger than the spin–orbit parameters in $\hat{H}_{eff}$. This is the important consideration when treating the spin–orbit interaction as small compared to E_{JT} and justifies the approach here.

Finally, we consider the intensity in the origins. The observed oscillator strength is 5×10^{-9}. To estimate the total magnetic dipole intensity in the vibrational progressions, we multiply this by the intensity ratio between the t_{1u} and t_{2u} false origins and the progressions in a_{1g} and e_g built on them, about 1:100. The total observed magnetic dipole intensity is then about 5×10^{-7}. We can calculate the magnetic dipole intensity using the eigenvectors of the crystal field calculation. Taking the refractive index to be 1.5 and the orbital reduction factor as 0.4, a value which seems appropriate in $CrCl_6^{3-}$,[11] the calculated intensity is 6×10^{-6}. The disagreement may be in part due to the Cr^{2+} content of the crystal leading to an overestimation of the Cr^{3+} concentration. The total intensity of the $^4T_{2g}$ transition in the absorption spectrum is 2.2×10^{-5}. This value is somewhat lower than the $^4A_{2g} \rightarrow {}^4T_{2g}$ intensities usually found in octahedral chromium(III) complexes; e.g., in chrome alum, an intensity of 1.6×10^{-4} has been reported.[12] This tends to support the idea that the measured intensity may be too low.

Conclusion

We have demonstrated the existence of a Jahn–Teller interaction in the $^4T_{2g}$ state of $CrCl_6^{3-}$ in $Cs_2NaInCl_6$ by observation of a Ham effect and a progression in an e_g mode in the luminescence spectrum. As far as the relative contributions of t_{2u}, t_{1u}, and t'_{1u} modes to the vibronic intensity mechanism of the $^4A_{2g} \leftrightarrow {}^4T_{2g}$ transition are concerned, our results are in good agreement with the results of a moment analysis of MCD measurements.[1,2] On the other hand, our interpretation in terms of a Jahn–Teller effect is at variance with the current interpretation of the MCD data.[1,2] No spectra on oriented crystals have been measured, however; and the Zeeman effect is expected to be anisotropic.[3]

Acknowledgment. We acknowledge the Swiss National Science Foundation for grants for equipment and support (T.R.S.). We thank R. G. Denning for helpful collaboration, W. Yeakel and E. R. Krausz for useful comments, and S. Fehr for the chromium analysis.

Registry No. $CrCl_6^{3-}$, 15276-03-6; $Cs_2NaInCl_6$, 32201-16-4.

References and Notes

(1) R. W. Schwartz, *Inorg. Chem.*, **15**, 2817 (1976).
(2) P. Shaw, Ph.D. Thesis, Oxford, 1975.
(3) M. D. Sturge, *Phys. Rev. B*, **1**, 1005 (1970).
(4) P. J. Stephens and Marian Lowe-Pariseau, *Phy. Rev.*, **171**, 322 (1968).
(5) L. R. Morss, M. Siegal, L. Stenger, and N. Edelstein, *Inorg. Chem.*, **9**, 1771 (1970).
(6) R. G. Denning, private communication.
(7) F. S. Ham, *Phys. Rev.*, [*Sect.*] *A*, **138**, 1727 (1965).
(8) M. D. Sturge, *Solid State Phys.*, **20**, 91 (1967).
(9) D. L. Wood, J. Ferguson, K. Knox, and J. F. Dillon, *J. Chem. Phys.*, **39**, 890 (1963).
(10) C. J. Ballhausen, *Theor. Chim. Acta*, **1**, 285 (1963).
(11) M. Mayer and H. Szynczak, *Phys. Status Solidi B*, **62**, 721 (1974).
(12) N. S. Hush and R. J. M. Hobbs, *Prog. Inorg. Chem.*, **10**, 259 (1968).

Contribution from the Department of Chemistry,
University College, Dublin, Ireland

Molecular Orbital Theory of Organometallic Compounds. 15.[1] A Comparative Study of Ferrocene and π-Cyclopentadienyl-(3)-1,2-dicarbollyliron

DAVID A. BROWN,* M. O. FANNING, and N. J. FITZPATRICK

Received September 23, 1977

The SCCC MO method is used to compare the electronic structures of π-cyclopentadienyl-(3)-1,2-dicarbollyliron and its carbon analogue, ferrocene. It is shown that while the bonding in ferrocene involves primarily the π orbitals of the cyclopentadienide ring, that in the dicarbollide complex involves the σ orbitals in an important role; thus, the intuitive view that the frontier orbitals on the dicarbollide ligand are directly comparable to the π orbitals of the cyclopentadienide ligand requires an important qualification. In both complexes the HOMO's have very high d_{z^2} character. In the dicarbollide complex the dianionic dicarbollide and anionic cyclopentadienide ligands donate 1.037 and 0.164 electrons to the iron(II) atom. Agreement between calculated results and experiment in closely related systems is noted.

Introduction

One of the most interesting developments in the field of organometallic chemistry has been the isolation of an extensive series of metallocarborane complexes.[2] A common feature of these complexes involves the bonding of a range of polyhedral carboranes to a transition metal via direct interaction between the metal and a nearly pentagonal open face of the carborane, e.g., as in $[Fe(C_2B_9H_{11})_2]^{2-}$. An extensive series of mixed metallocarborane complexes in which a transition metal is bonded on one side to a carborane and on the other to more conventional π ligands such as cyclopentadienyl or carbon monoxide as in $[(C_2B_9H_{11})Fe(C_5H_5)]^-$ and $[(C_2B_9H_{11})Mn(CO)_3]^-$ also exists.

In view of the extensive studies of these systems, it is surprising that little attention has been paid to detailed discussion of the bonding in the metallocarboranes and, in particular, to the similarities and differences between them and the closely related carbon analogues, e.g., ferrocene;

0020-1669/78/1317-1620$01.00/0